

1 A uniaxial cyclic compression method for characterizing the rheological behavior
2 of mechanically dewatered sewage sludge

3 *Fenglin Liang¹, Martial Sauceau¹, Gilles Dusserre² and Patricia Arlabosse¹*

4 Corresponding author: Patricia.Arlabosse@mines-albi.fr

5 ¹*Université de Toulouse; Mines Albi; CNRS; Centre RAPSODEE, Campus Jarlard, 81013 Albi, France*

6 ²*Université de Toulouse; CNRS, Mines Albi, INSA, UPS, ISAE-SUPAERO; ICA (Institut Clément Ader);
7 Campus Jarlard, F-81013 Albi, France*

8 **Abstract**

9 The mechanically dewatered sewage sludge with total solid content around 20% on a weight basis is
10 very similar to yield stress fluid, its complex transition between solid and fluid states is not perfectly
11 reversible and especially challenging in terms of pumping, land spreading and drying. To characterize
12 the rheological and textural properties of highly concentrated sludge, a specific methodology based
13 on uniaxial single and cyclic compression tests is developed. Three types of sludge samples (fresh
14 original, fresh premixed and aged original ones) are extruded into cylinders and pressed between
15 two parallel plates using a material testing machine. In single compression, the bioyield point is
16 around 7.3 kPa with true strain equal to 0.21 beyond which the sludge fractures. The cyclic
17 compression tests reveal that the sludge behaves as a viscoelastic body when the true strain is
18 smaller than 0.05. Once exceeding the yield stress, it behaves as a visco-elasto-plastic one. The
19 elastic module is around 78 kPa; the viscosity is deduced, in the order of magnitude 10^4 to 10^5 Pa.s
20 and the yield stress is estimated about 4 kPa. In the unloading phase, the sludge behaves again as a
21 viscoelastic body with clear hysteresis. With the increase of compression speed, the viscosity
22 declines. This confirms that the sludge is a shear-thinning material. The yield stress and the bioyield
23 increase with compression speed, but it does not induce extra internal damage in the samples since
24 the resilience and the cohesiveness are unaltered. The reliability and sensitivity of the method is
25 justified by highlighting the changes of sludge behavior induced by aging and premixing: both
26 decrease the strain energy density, but do aggravate the adhesiveness of the sludge; the aging makes
27 the sludge less cohesive, while the premixing does not modify its cohesiveness. In spite of changes in
28 test conditions, the elastic module of sludge samples remains unchanged.

29 **Keywords**

30 Rheology, visco-elasto-plastic, yield, texture, aging, premixing

31 1 Introduction

32 In volume, sewage sludge is the largest by-product recovered in a municipal wastewater treatment
33 plant (WWTP). Typically, these solids and biosolids are in the form of a liquid or semisolid liquid,
34 which contain from 0.25 to 5% of solid by weight. Thickening, conditioning and mechanical
35 dewatering are necessary treatments to remove the moisture, which reduces the volume, improves
36 the handling, facilitates the storage and decreases the transport costs for further valorization. In
37 Europe, most of the municipal WWTPs implement these treatments to best achieve a total solid
38 content (TS) around 18 to 25% with a continuous dewatering process. Most of the dewatered sludge
39 maintains its shape in the same way as a solid under the effect of gravity but is able to flow like a
40 fluid, i.e. a substance that continuously deforms, when submitted to a high enough stress. These soft
41 materials are very similar to yield stress fluids. But the key difference is that the highly concentrated
42 sludge cannot recover the properties it had before flowing in the liquid regime: the transition
43 between solid and fluid states is not perfectly reversible (Coussot, 2014). Sludge processing, reuse
44 and disposal are among the most complex technical problems facing the engineers in the field of
45 wastewater treatment. This complex transition between solid and fluid states is especially
46 challenging in terms of pumping, land spreading and drying (Baudez et al., 1998). Concurrently, the
47 inevitable impacts of aging (due to the degradation of organic matters) and premixing (including
48 shearing, pressing and squeezing induced by pumping, transporting and other mechanical handlings)
49 modify more or less the rheological and textural behaviors of sludge. Papadakis and Bahu (1992)
50 reported the crucial sludge stickiness to equipment surfaces observed in drying processes. The
51 sticking accumulation may lead to significant reduction of dehydration capacity and efficiency
52 (Beckley and Banerjee, 1999; Jing et al., 1999; Kudra, 2003; Ohm et al., 2009). Therefore, the
53 characterization of rheological and textural behaviors of mechanically dewatered sewage sludge is
54 aimed to settle the dominant properties with respect to operational conditions so as to optimize the
55 processing design.

56 The main factors dominating the sewage sludge properties are the temperature (Lotito and Lotito,
57 2014; Feng et al., 2014; Dai et al., 2014; Battistoni, 1997; Baroutian et al., 2013; Baudez et al., 2013;
58 Farno et al., 2014; Mori et al., 2006), the composition and the microstructure (Ruiz and Wisniewski,
59 2008; Lin et al., 2013; Nielsen et al., 1996; Pevere et al., 2009; O’Kelly, 2008; Baudez and Coussot,
60 2001; Baudez, 2008; Agoda-Tandjawa et al., 2013; Mori et al., 2008; Ma et al. 2014) as well as the
61 solid concentration. Until 2013 (Seyssiecq et al., 2003; Eshtiaghi et al., 2013), most of the rheological
62 characterization studies were focused on sludge in liquid to pasty states ($1.5\% < TS < 15\%$).
63 Rheometers have always been the mainstream tool. Unfortunately, an effective standard specifically
64 designed for sludge, that includes both sample preparation and characterization, is lacking.
65 Considering the large number of operating parameters, such as the geometry, gap size, wall surface
66 roughness and pre-shearing rate, it is not possible to get an absolute value for the viscosity
67 (Ratkovich et al., 2013) and the yield stress (Jiang et al., 2014). Few publications are devoted to the
68 characterization of pasty sludge having TS higher than 15%. Jiang et al. (2014) carried out both steady
69 flow and dynamic oscillatory measurements to investigate the impact of both solid content and
70 temperature. These measurements were all conducted on a conventional rotating rheometer. Even
71 at $TS=16\%$, the sludge was flowable under tangential stress. The same observation was reported by
72 Agoda-Tandjawa et al. (2013). For another sludge at TS around 21.5%, Charlou (2014) reported a
73 fracturing phenomenon in a horizontal plane using a parallel plate rheometer in oscillation mode.
74 The shearing test was inadequate to characterize this sludge. However, Battistoni (1997) succeeded
75 in investigating the rheological properties of highly concentrated sludge (up to $TS=33\%$) with a
76 coaxial cylindrical geometry. But, prior to the rheological test, the sludge was sieved (with a No. 20
77 U.S. standard sieve of 0.841 mm) and sheared at a shearing rate of 100 s^{-1} for 4 minutes. These pre-
78 treatments not only irreversibly altered the composition, but also the microstructure of the sludge
79 and the moisture distribution (Liang et al., 2016). It therefore seems that rotational rheometers have
80 limited interest when working with a mechanically dewatered sludge.

81 Alternative methods are reported in the literature. Ruiz and Wisniewski (2008) and Ruiz et al. (2010)
82 adopted the Atterberg Limits, widely applied in civil engineering, to correlate the rheological
83 characteristics of the sludge to its drying and shrinkage aptitudes. O’Kelly (2005; 2006) applied
84 triaxial compression tests, commonly used in soil mechanics, to simulate the mechanical and
85 geotechnical behaviors of solid sludge around TS=55% for landfilling purposes. Unfortunately, these
86 methods are not suitable for the purpose of determining the rheological properties of highly
87 concentrated sludge. In another scientific area, G’sell and Jonas (1979) proposed a tensile testing at
88 constant local true strain rate to determine the plastic behavior of solid polymers with True strain-
89 True stress curves. Ramírez-Wong et al. (1996) used the squeezing flow viscometry technique and
90 the definition of true strain and true stress to evaluate the rheological properties of fresh corn masa
91 while S. Sharma and Bhattacharya (2014) adopted this method to show the fracture characteristics of
92 model food gels. These studies share the common features of involving pasty, gelatinous or solid-like
93 materials and compressing it between two parallel plates to provide an accurate measure of the
94 material behavior during the test. Suitable for application in different fields, universal testing
95 machines (UTM), also known as material testing machines, can perform many standard tests, including
96 single and multiple cycle compression, tensile strength, creep, stress relaxation, resiliency, to
97 describe the deformation behavior and creep properties of materials. UTM have also been marketed
98 to specific sectors with specialized name (texture analyzer for food and top load compression tester
99 for packaging, for instance). Thus, by referring to conventional uniaxial compression tests used for
100 characterizing somewhat similar materials in various fields of research, such as single sludge granules
101 (Lin et al., 2013), gels (Sharma and Bhattacharya, 2014; Yu et al., 2012), sandstones (Zhang et al.,
102 2014) and asphalt mixtures (Cai et al., 2013), we developed an entire methodology - from
103 experiment to modelling till simulation - to describe the deformation and flow of a mechanically
104 dewatered sewage sludge (i.e. at TS around 20%) under a given mechanical load.

105 For the characterization of sludge stickiness, Peeters et al. (2010) and Li et al. (2014) adapted the
106 shearing test used in powder engineering to map the adhesive and cohesive stresses of sludge at
107 increasing solid content. However, these tests only provided sticky strength under shearing. The
108 other textural properties as strain energy density, resilience, energy of adhesion and cohesiveness
109 for energy consumption analysis stayed unknown. The lack of these primary elements led us to adopt
110 the entire analysis of texture, also using uniaxial cyclic compression test, developed in food
111 engineering (Steffe, 1996; Hort et al., 1997) for better understanding of sludge behavior.

112 The present paper focuses on the experimental methodology only. The objective is first to analyze
113 the rheological and textural behavior of the material, such as elasticity, viscosity, plasticity, hardening
114 index and adhesive and cohesive parameters, under different types operational conditions. In a
115 second part, particular emphasis is being placed on the reliability and sensitivity of this method that
116 are justified by highlighting the changes induced by aging and mixing. This methodology is realised
117 under uniaxial compression, so that it can be applied to sludge behaving as a soft solid with TS
118 between the liquid limit (evaluated by slump test and/or ASTM D 4318 to ensure that the sludge
119 sample can not flow with its own weight under gravity) and the plastic limit (ASTM D 4318 to ensure
120 that it can be considered as a continuous medium).

121 **2 Material and method**

122 **2.1 Origin of the sewage sludge**

123 The sewage sludge was collected at the WWTP of Albi city in France. Before the biological treatment,
124 the wastewater is screened, de-sanded and de-oiled (**Figure 1**). After the extended aeration, a post-
125 treatment removes the nitrogen and the phosphorus from the effluent. The excess sludge is
126 flocculated with a high cationic polymer (BASF Zetag® 8868), thickened and anaerobically digested
127 for six weeks. The digested sludge is flocculated again with a second high cationic polymer (BASF
128 Zetag® 9018) and mechanically dewatered in centrifuges. The material used in this study was

129 sampled after the centrifugation. Sludge composition was analyzed according to standard EN
130 12880:2000. The sample ranged in dry matter content from 18.5 to 21 wt%.

131 **Figure 1**

132 As the sludge contains active organic matter, it is necessary to avoid biodegradation phenomena
133 (aging) to have a chance of getting repeatable tests. Storing the sludge in a sealed barrel avoids
134 water evaporation only. O’Kelly (2008) characterized the composition of a sludge sample kept at
135 atmospheric conditions in a sealed barrel for 13 years: the TS only increased from 12% to 13% while
136 the total volatile solids significantly decreased from 70% to 55%. To block the biological activity, F.
137 Chaari et al. (2003) added chemical reagents into the sludge and kept it in a fridge. Ma et al. (2014)
138 refrigerated sludge at 4°C for one night. Nevertheless, by surveying the composition changes in
139 extracellular polymeric substances, Nielsen et al. (1996) proved that the sludge biodegradation was
140 mostly active during the first three days of storage and tended to be stable beyond 12 days. So,
141 Curvers et al. (2009) stored the sludge at 4°C for 14 days, while Baudez et al. (2013; 2011) have
142 chosen a refrigerating storage of 30 days before testing. In this study, the sludge was immediately
143 transported to the laboratory within one hour after sampling and divided into two samples. To
144 prevent any aging effect, one was prepared immediately for testing while the second one was kept at
145 4°C for 6 days to investigate the influence of aging.

146 **2.2 Sample preparation**

147 Inherently, the sludge is an extremely heterogeneous material, whatever the observation scales. To
148 be representative, a large sample is thus required. Furthermore, shaping the material into cylinder is
149 needed for the test purpose. To have a chance to get a repeatable and reproducible protocol, three
150 methods of preparation are tested and compared: (i) use of a cookie-cutter for shaping the raw
151 sludge, (ii) manual extrusion of the raw sample and (iii) homogenization of the raw sludge with an
152 automatic planetary mixer prior to the manual extrusion. The cylindrical cookie-cutter is pressed into
153 the pasty sludge and then retrieved with a pre-formed piece of sludge. The manual piston extruder
154 (**Figure 2 (a)**) is made up of a rack connected to a piston, a pinion connected to a crank (by which the
155 torque is converted into a linear force on the piston while meshing the rack with the pinion), and a
156 cylindrical recipient (13 cm in diameter). The sludge is pressed through a subconical tube, 3.4 cm in
157 diameter, by the linear force. The extrusion can slightly homogenize a mass of sludge without
158 changing its microstructure much. However, preshearing is widely used before testing in flowable
159 sewage sludge rheological characterization on a conventional rheometer (Dai et al., 2014; Battistoni,
160 1997; Baudez et al., 2011; Markis et al. 2014). The aim is first to homogenize the sample, which is all
161 the more critical than its volume is small (around 0.4 mL), but also to erase the material memory. As
162 the size of our samples is quite large (around 46 mL), an automatic planetary mixer (Dito Sama,
163 Sensils, France) is used to smash the polymer blobs and homogenize the original material.

164 **Figure 2**

165 A typical photo of the material after mixing and extrusion is shown on **Figure 2 (c)**. Compared to the
166 raw material (**Figure 2 (b)**), its physical appearance is very different, smoother and shinier.

167 For each preparation method, the size and the weight of at least three cylindrical sludge samples is
168 measured and the bulk density deduced. Neither significant loss in mass, nor remarkable gain in TS
169 (about 0.2%) was observed after premixing. Assessment of the sample homogeneity after shaping is
170 based on the calculation of the standard deviation of the bulk densities. The average densities and
171 the associated standard deviations are listed in the **Table 1** for the three preparation methods.

Preparation method	Bulk density average (kg/m ³)	Standard deviation (kg/m ³)	Deviation percentage (%)
Cookie cutter	948.5	34.7	3.7

Extruder	1061.8	13.9	1.3
Mixer & extruder	1046.5	12.7	1.2

Table 1: Influence of sample preparation methods on averaged bulk density and standard deviation

The bulk density of samples shaped by cookie cutter is lower than that of water, because the incorporation of air within the loosened sludge. Extrusion reduces the material porosity and leads to denser samples. In addition, the extruded samples are more homogeneous than those made by using a simple cookie cutter. Premixing (10 min at about 1232 rpm) strengthens these trends. However, direct observation highlights that the premixed sludge is actually much more sticky than the original material. This phenomenon was also observed by Charlou (2014). To expect a repeatable and reproducible characterization method, extrusion is selected as the best method for preparing solid-like sludge samples. All the extruded sludge samples have the same dimensions, $r_0 = 17$ mm and $h_0 = 51$ mm, so the aspect ratio is $2r_0/h_0 = 1.5$. Aging and premixing are considered as two operating parameters, whose influence has to be tested. Further more, as the sludge is extruded into cylinders, the sludge on the surface of the shaped cylindrical samples is somewhat sheared, pressed or squeezed. The premixing test is thus indispensable to verify whether the sample shaping by extrusion is reliable and applicable or not.

All the experiments are carried out in the air-conditioned laboratory (21°C). The TS of sludge is surveyed before sample preparation and after compression test in order to verify that the water evaporation is negligible and has no impact of the measurement.

2.3 Uniaxial compression at different velocities or deformations

All the mechanical tests described in the following are carried out with the material testing machine (UTM) LRX Plus of Lloyd Instrument (Elancourt, France) with capacity up to 5 kN. The UTM (**Figure 3**) includes a control console, a fixed worktable, a single column with a crosshead travel range of 735 mm embedded with an interchangeable mobile load cell equipped with a force sensor of 50 N. The uniaxial compression tests are configured at a constant crosshead displacement speed V (mm/s), either with a maximal loading force F_{\max} (N) or a maximal sample change in height Δh_{\max} (mm). During the experiment, the force F (N), the time t (s), and the crosshead displacement (namely the change in height of the sludge sample) Δh (mm), are recorded on a computer.

Figure 3

Three different types of mechanical tests were performed:

- Single compression tests on fresh raw sludge samples with $\Delta h_{\max} = 35$ mm and $V = 0.5$ mm/s, to define the bioyield point which is related to a failure in the microstructure of the material and also known as the fracturability (Pelletier et al., 1998; Mohsenin, 1984);
- 1 cycle (loading-unloading) compression tests on fresh raw sludge samples with different maximal deformations ($\Delta h_{\max} = 1, 2, 3$ and 10 mm) at fixed compression speed $V = 0.5$ mm/s - the upstroke phase occurs once the crosshead reaches the preset Δh_{\max} - to identify the rheological behavior of the material under 1 cycle of loading and releasing manipulations;
- 2 consecutive cycles (loading-unloading) compression tests on three types of samples (fresh raw, fresh destructured and aging raw) with different compression speeds ($V = 0.5, 1.0$ and 1.5 mm/s) at fixed maximal deformation $\Delta h_{\max} = 10$ mm to determine the rheological behavior and textural properties of the material under 2 cycles of loading and releasing manipulations (Pelletier et al., 1998).

For each input condition at least three samples are characterized.

212 3 Calculations of mechanics and texture quantities

213 3.1 True stress and true strain

214 A typical force measured in response to a cyclic mechanical compression test with pre-set maximal
215 deformation (here $\Delta h_{\max}=35$ mm) and crosshead displacement speed (here $V=0.5$ mm/s) is plotted
216 over time in **Figure 4**.

217 **Figure 4**

218 In order to interpret the rheological behavior of the sludge sample, the true stress σ (Pa), and the
219 true strain ε (-), are computed from the instantaneous force F , the cross-sectional area S (m^2), and
220 the deformation Δh . We assume (i) that there is no friction at the contact surface between the
221 sample and the UTM plates (ii) that the cylindrical sludge sample is incompressible (The bulk volume
222 of cylindrical samples measured before and after compression test is almost unchanged.). So the
223 samples can keep their cylindrical shape during the compression tests. Of course, the side surface of
224 the sample is slightly curved after the compression test. However, the ratio of diameters between
225 the sections of higher and lower radii is about 1.07, and the discrepancy between the original size
226 and the final one is less than 10%, as can be seen on **Figure 6**, thus this assumption seems quite
227 acceptable.

228 Since the extruded cylindrical sample is considered incompressible during a trial, the instantaneous
229 cross-sectional area $S(t)$ can be calculated according to the conservation of the sample's volume:

$$230 \quad S(t) = \pi r(t)^2 = \frac{h_0}{(h_0 - \Delta h(t))} \pi r_0^2 \quad (1)$$

231 Where $r(t)$ is the sample's radius at time t .

232 The previous assumption of sliding without friction during uniaxial compression leads to a uniform
233 and uniaxial stress field. The true stress σ is thus expressed as the force $F(t)$ divided by the
234 instantaneous cross-sectional area $S(t)$:

$$235 \quad \sigma(t) = \frac{F(t)}{S(t)} = \frac{(h_0 - \Delta h(t))}{h_0} \cdot \frac{F(t)}{\pi r_0^2} \quad (2)$$

236 The axial true strain increment $d\varepsilon$ is defined as the height increment dh divided by the instantaneous
237 height $h(t)$: $d\varepsilon = \frac{dh}{h(t)}$. Therefore, the axial true strain $\varepsilon(t)$ is calculated as follows:

$$238 \quad \varepsilon(t) = \ln\left(\frac{h_0 + \Delta h(t)}{h_0}\right) \quad (3)$$

239 In the following, all the experimental data are converted into true stress and true strain (often called
240 stress and strain for short).

241 3.2 Strain energy density and resilience

242 It is assumed that there is no friction on contact surfaces, so it is considered that there is no energy
243 dissipated by friction in these tests. The energy introduced into the material due to the loading is
244 therefore assimilated to the strain energy. The strain-energy density of the material u (J/m^3)
245 corresponds to the normalized strain energy by unit volume that is needed to achieve a certain
246 deformation. It is equal to the area under the stress-strain diagram:

$$247 \quad u = \int_{\text{loading}} \sigma d\varepsilon \quad (4)$$

248 If the material is not perfectly elastic, only part of the strain energy can be recovered after the load is
 249 removed. The recoverable part is the resilience of the material u_r (Roudot, 2002). u_r is equal to the
 250 area of the stress-strain curve during unloading:

$$251 \quad u_r = \int_{\text{unloading}} \sigma d\varepsilon \quad (5)$$

252 Where u_r is also expressed in J/m^3 .

253 Finally, the difference $u-u_r$ gives the energy density that is irreversibly stored or dissipated within the
 254 sample, as permanent deformation, heat or cracking, during a loading-unloading application. A ratio
 255 between unrecoverable energy and strain energy, e (%), can be obtained as follows:

$$256 \quad e = \frac{u-u_r}{u} \quad (6)$$

257 3.3 Texture profile analysis

258 In food science, double compression tests are recognized as an instrumental means of characterizing
 259 the texture of the material (Steffe, 1996). Usually, the sample is compressed two times, up to 80% of
 260 its original height, with the UTM. Several textural parameters can be deduced from the texture
 261 profile curve. This curve represents the evolution of the force over the time. Three of them are of
 262 particular interest for sludge treatment - adhesive strength, energy of adhesion and cohesiveness -
 263 since the adhesion to the filter clothes during mechanical dewatering, to the dryer walls during
 264 thermal drying or to the chopping blades of stirring device in solar dryers is very common in sludge
 265 treatment. A product with strong cohesion will be more tolerant of manufacturing.

266 The adhesive strength $F_{ad,max}$ is the maximum negative force. Knowing the contact surface, the
 267 adhesive stress $\sigma_{ad,max}$ can be calculated. The energy of adhesion w_{ad} represents the mechanical work
 268 caused by a tensile force to separate the material from the plate. w_{ad} , expressed in J, corresponds to
 269 the area under the zero force line after the compression:

$$270 \quad w_{ad} = \int_{\text{adhesion}} FVdt \quad (7)$$

271 Where F is the adhesive force measured between the two cycles and Vdt is the displacement
 272 increment. The values of adhesive strength and the energy of adhesion are negative, absolute
 273 numbers will be reported in **Table 2 to 5**.

274 The cohesiveness co , a dimensionless quantity, corresponds to the ratio of the mechanical work
 275 done by the compression force during the second compression w_2 to the mechanical work done by
 276 this force during the first compression w_1 . The cohesiveness is used to evaluate how well the
 277 material withstands a second deformation relative to its resistance under the first deformation. It is
 278 calculated as follows:

$$279 \quad co = w_2/w_1 \quad \text{with } w_k = \int_{k^{\text{th}} \text{ cycle}} FVdt \quad (8)$$

280 Where k is the k^{th} compression cycle.

281 4 Results and discussion

282 4.1 Identification of rheological and textural properties

283 The TS of tested sludge samples are 18.86% before shaping preparation and 19.37% after
 284 compression test. This increase of 0.5% in TS due to water evaporation is negligible. The
 285 experimental results are therefore reliable for sludge behavior interpretation.

286 4.1.1 Identification of the bioyield point through simple compression

287 The mechanical responses of three sludge samples, directly shaped into cylinder by extrusion, to a
288 single loading phase are plotted in **Figure 5 (a) (b)**. The experiment was performed at $V = 0.5$ mm/s
289 with $\Delta h_{\max}=35$ mm. Results are very well repeatable with a clear trend. A curve such as the one
290 illustrated in **Figure 5 (a) (b)** is typical for solid foods, biological solids (Steffe, 1996) but also for solid
291 polymer (G'sell and Jonas, 1979). The flocculation of municipal sewage sludge particles is a decisive
292 step in sludge processing. The high cationic polymer forms the sludge structure with a good
293 mechanical strength (Agoda-Tandjawa et al., 2013; Wolny et al., 2008). This may be one of the
294 essential reasons that explain the similarity of the rheological behavior of these materials.

295 **Figure 5**

296 Except near the origin ($\varepsilon < 0.015$) where the curve is concave, the initial part of the curve is almost a
297 straight line up to the limit of linearity (around $\varepsilon = 0.05$). The concavity may result from three reasons:
298 the non-parallelism of contact surfaces, which is a default of sludge samples; the rearrangement of
299 the skeleton (some kind of collapse) owing to the applied stress; and the sludge adhesion to the
300 contact surface of load cell. These phenomena are very common. For instance, Johnson et al. (1971)
301 pointed out the significance of attractive surface under light load with soft materials. Sharma et al.
302 (2011) also observed it when compressing human and animal lenses. Consequently, the data in this
303 concave range will not be exploited for further behavior analysis.

304 The apparent elastic modulus, slope of stress-strain curve in the linear range ($0.015 < \varepsilon < 0.05$), is often
305 considered as an index of firmness. For these specific conditions, the estimated value is
306 78.2 ± 9.0 kPa. This order of magnitude is quite close to the elastic modulus of gelatin gel, of some
307 rubber or banana (Chhabra and Richardson, 2011) and that of concentrated premixed sludge
308 (TS $\approx 17.4\%$) (Ségalen et al., 2015). For $\varepsilon > 0.05$, the stress continues to increase with the progress of
309 loading, however, the slope starts to decrease, which indicates the deferred behavior of viscoelastic
310 property.

311 The stress reaches the maximum value around $\sigma_c = 7300$ Pa at $\varepsilon_c = 0.21$. This maximum, called the
312 bioyield point, reflects the sensitivity of the biomaterial to irreversible internal damage. Beyond this
313 point, the stress decreases with increasing strain. The machine actually measures the propagation of
314 micro-fractures. The data can no longer provide direct access to the intrinsic properties of sludge
315 samples. Therefore, the strain range will be limited to 0-0.21 in the following cyclic compressions.

316 During the mechanical tests, only external fissures or fractures can be seen. In order to ensure that
317 there is no internal fissures or fractures, after the test, free of external cracks samples are cut into
318 slices. Only the samples without evident cracking are kept for further data analysis (**Figure 6**).

319 **Figure 6**

320 4.1.2 Identification of the rheological behavior through cyclic compressions

321 The stress-strain curves for a loading-unloading cycle with maximum deformations $\Delta h_{\max}=1, 2, 3$ and
322 10 mm and $V=0.5$ mm/s are plotted in **Figure 5 (c)**. In the loading phase, the curves are well
323 superposed, in the unloading phase, the curves for $\Delta h_{\max}=1$ and 2 mm display very rapid recovery at
324 the end parts in comparison with those for $\Delta h_{\max}=3$ and 10 mm. It might be inferred that there is a
325 change of regime between the maximum stress values of $\Delta h_{\max}=2$ and 3 mm, namely between 2300
326 and 4100 Pa.

327 When the compression starts, the concavity of the loading curves is observed again in the range up
328 to about $\varepsilon_A = 0.01$ and $\sigma_c = 7300$ Pa.

329 For $\Delta h_{\max}=1$ mm, a half of the data in loading phase is within this range. So only the data in the
330 unloading phase are effective for behavior analysis. As can be seen on **Figure 5 (c)**, the slope of
331 stress-strain curve decreases, this means that the recovery speed of the material increases. Plus, the
332 sludge can almost completely recover itself. Hence, sludge samples exhibit a viscoelastic behavior at
333 small deformation. As the relaxation time of this viscoelastic body, defined as the ratio of its viscosity
334 to its elastic modulus, is the same order of magnitude as the unloading time in this test (2 s), we can
335 then estimate that the order of magnitude for the sludge viscosity is 10^4 to 10^5 Pa.s. This value is very
336 close to the viscosity of borosilicate glass at 900 °C (Dusserre et al., 2011).

337 For $\Delta h_{\max}=2$ mm, a quarter of data in the loading phase is influenced by the curve concavity.
338 Accordingly, the data in the unloading phase are main reference for analysis. A small residual
339 deformation of 0.87 mm ($\varepsilon=0.0169$) is measured. However, as this value is in the concave range of
340 $\varepsilon<0.01$, it is hard to define whether this residual deformation is generated by plastic property or if it
341 is just the initial distance between the contact surfaces of the material and the load cell. Thus, it is
342 still the viscoelastic property that dominates the sludge behavior in this test.

343 For $\Delta h_{\max}=3$ and 10 mm, the hysteretic behavior between loading and unloading curves become
344 more evident. The residual deformations are 1.13 mm ($\varepsilon=0.0219$) and 6.04 mm ($\varepsilon=0.119$),
345 respectively. The strains are out of the range of the concavity, so these irreversible deformations
346 should be the plastic effect of sludge samples. This confirms that the yield stress is exceeded in the
347 test for $\Delta h_{\max}=3$ mm. Above the threshold, the change of regime takes place, the material undergoes
348 plastic deformations and the slope of stress-strain curves decreases much more significantly with the
349 downstroke. For $\Delta h_{\max}=10$ mm, by the end of loading phase ($0.19<\varepsilon<0.21$), the stress varies very little
350 (from 6477 to 6542 Pa), the sludge's behavior is very similar to a plastic flow. The sludge sample
351 behaves like a viscoelastic body, again, in unloading phase.

352 The previous four tests are carried out with fixed crosshead displacement speed $V=0.5$ mm/s and
353 different maximal deformations Δh_{\max} ; in the following characterizing measurements, Δh_{\max} is fixed
354 to 10 mm with V preset at 0.5, 1.0 and 1.5 mm/s. The stress-strain curves for two loading-unloading
355 cycles are plotted in **Figure 5 (d)**.

356 At the beginning of the compression, the concavity of curves persists. For $0.01<\varepsilon<0.03$, the material
357 response is nearly rate-independent. In this strain range, the effect of viscoelasticity is not yet
358 notable, plus the elastic behavior is independent of compression speed, so the curves are almost
359 linear in this part. The elastic property prevails until $\varepsilon_E=0.03$ and $\sigma_E=2000$ Pa. The impact of
360 crosshead displacement speed V becomes remarkable with growing influence of viscoelasticity effect:
361 to achieve the same deformation $\varepsilon=0.01$, it requires higher stress for higher compression speed test:
362 6403 Pa (13% higher) for $V=1.5$ mm/s; 5896 Pa (4% higher) for $V=1.0$ mm/s in comparison with
363 5667 Pa for $V=0.5$ mm/s. This increase in stress with the augmentation of compression speed
364 confirms the existence of viscous property in sludge samples.

365 According to the Newton's law, the stress is proportional to the strain rate when the viscosity is
366 constant, however, at $\varepsilon=0.1$, the strain rates are 0.0326 s^{-1} , 0.0217 s^{-1} and 0.0109 s^{-1} , respectively.
367 The corresponding stress value is not in proportion with the increase of strain rates. The sludge
368 samples exhibit therefore a shear thinning property as widely reported (Jiang et al., 2014; Mori et al.,
369 2008; Ma et al., 2014; Markis et al., 2014).

370 To estimate the order of magnitude of the yield stress (see **Figure 5 (d)**), two regression lines are
371 plotted: one is regressed with the data in the range $0.01<\varepsilon<0.03$, this line simulates the ideal elastic
372 behavior of the material; the other is regressed with the data by the end of loading $0.19<\varepsilon<0.21$, to
373 simulate the ideal plastic behavior of the material. The intersection of these two lines corresponds to
374 the critical strain around $\varepsilon_c=0.08$, the yield stress is therefore estimated to be around 4600 Pa for

375 V=0.5 mm/s, 4950 Pa for V=1.0 mm/s and 5700 Pa for V=1.5 mm/s. Not only the viscosity, but also
 376 the yield stress is very dependent on the compression speed. Above this critical yield stress, the
 377 sludge goes through large deformations including elastic, viscous and plastic ones. The sludge
 378 samples behave as a visco-elasto-plastic body to the end of loading phase.

379 Once the crosshead displacement has reached the pre-set maximal deformation, the discharging
 380 phase starts. At the end of the discharging process, the strain is non-zero when the stress reaches
 381 zero. Thus, as expected following the charging cycle analysis, two types of deformations can be
 382 identified:

- 383 • A recoverable deformation, which might be induced either by the elasticity or the
 384 viscoelasticity of the sludge. The discharging curves show pure elastic response at the very
 385 beginning of the unloading phase (Sveegaard et al., 2012). But rapidly, the predominance of
 386 the viscoelastic recovery behavior of sludge appears, since an elastic material should have
 387 recovered itself linearly all along the discharging phase in accordance with the Hooke's law;
- 388 • And a permanent deformation mostly caused by its plastic property. This permanent
 389 deformation does not depend on the crosshead speed, as can be seen on **Figure 5 (d)**. The
 390 higher the viscosity, the longer the relaxation time needed for the material to recover itself.
 391 According to the experiment duration, the so-called permanent deformation is around
 392 5.3 mm ($\epsilon=0.11$).

393 Most of the viscoplastic deformation occurs during the first compression cycle and, if the material is
 394 loaded again, viscoelastic deformations prevail then. The concavity of the curve near the origin is
 395 clearly less marked. This highlights that the hardening during the first cycle is enough to protect the
 396 sludge sample from new irreversible (plastic) deformations.

397 4.1.3 Influence of the operating conditions on the resilience and textural properties

398 Energy input and output values as well as textural properties are reported in **Table 2**. With the
 399 augmentation of compression speed, the maximum density of strain energy and the maximum
 400 adhesive stress increase. But the resilience, the energy of adhesion and the cohesiveness of sludge
 401 samples remain the same.

V (mm/s)	u (J/m ³)	e (-)	$\sigma_{ad,max}$ (Pa)	w _{ad} (10 ⁻⁶ J)	co (-)
0.5	1055 ± 86	75.3 ± 1.2%	195 ± 63	88.5 ± 5.9	47.5 ± 1.9%
1.0	1099 ± 28	75.3 ± 0.8%	242 ± 50	85.4 ± 29.3	48.2 ± 1.0%
1.5	1177 ± 38	75.4 ± 1.0%	310 ± 37	119.0 ± 8.4	47.7 ± 1.3%

402 **Table 2:** Calculated textural properties of sludge tested at increasing compression speed

403 4.2 Sensitivity of the method to highlight structural changes in the material

404 After mechanical dewatering, shearing and storing the sludge are almost unavoidable. It is well-
 405 known that both events have influences on the flow properties of the sludge (Kudra, 2003; Yen et al.,
 406 2002). They also have influences on its stickiness. Indeed, Charlou (2014) emphasized that a simple
 407 kneading makes the sludge sample significantly more adhesive than the raw one, without any change
 408 in solid content, temperature or composition. Both the microstructure (Charlou, 2014), characterized
 409 through the measurement of the particle size distribution, and the moisture distribution, measured
 410 by using low field ¹H nuclear magnetic resonance test, are modified (Liang et al., 2016). The final
 411 section of this paper examines the ability of this method to reveal changes in rheological properties
 412 induced by structural changes in the material.

413 4.2.1 Influence of aging

414 The stress- strain plots of three fresh sludge samples and three aged sludge samples (stored during 6
 415 days in a cold room at 4 °C) are plotted in **Figure 7**.

416

Figure 7

417 Aging does not have any significant effect on the apparent Young’s modulus. On the contrary, all the
 418 other rheological properties are very sensitive to the changes induced by the storage. The threshold
 419 stress corresponding to the limit between the viscoelastic and the viscoplastic domains decreases
 420 with aging. The raw sludge exhibits a viscoelastic behavior up to around $\sigma_p = 4600$ Pa while this
 421 threshold stress is around $\varepsilon_p=0.05$ and $\sigma_p = 3670$ Pa (about 20.2% lower) for the aged samples. At the
 422 end of the charging process, the maximum true stress is 6.4% lower for the aged samples. And finally,
 423 the permanent deformation is about 22.4% greater for the aged samples. From an energy point of
 424 view (see **Table 3**), the strain energy density u decreases with aging while the ratio e increases. As a
 425 result, the absolute total amount of energy dissipated within the material $u \bullet e$ is independent of
 426 aging. However, aging has a great influence on the textural properties of the material: the adhesive
 427 stress is doubled, the energy of adhesion increases more than 30 times and the sludge cohesiveness
 428 is reduced by 38.8%, emphasizing structural changes both at micro and macro scales.

Aging (day)	u (J/m ³)	e (-)	$\sigma_{ad,max}$ (Pa)	w_{ad} (10 ⁻⁶ J)	co (-)
0	1055 ± 86	75.3 ± 1.2%	217 ± 31	88.5 ± 5.9	63.9 ± 0.9%
6	991 ± 40	80.7 ± 0.9%	475 ± 52	2878.6 ± 331.5	39.1 ± 1.4%

429

Table 3: Calculatd textural properties of fresh and aged sludge samples

430 **4.2.2 Influence of mixing**

431 Before the mechanical test, two portions of sludge have been mixed for 5 and 20 min, respectively,
 432 at about 1232 rpm. The 5 minutes’ mixing is designed to reveal the impact of light destruction on
 433 sludge behavior with respect to the intense mixing for 20 minutes. The stress- strain plots of the raw
 434 sludge and the premixed samples are presented in **Figure 8**.

435

Figure 8

436 Mixing has nearly the same influence on the rheological properties as aging. The intense mixing (20
 437 min) has more important impact on sludge behavior than light mixing at 5 min. The sample shaping
 438 by extrusion causes simply very slight destruction on the surface of sludge cylinders, especially in
 439 comparison with 5 minutes mixing at 1232 rpm, it can thus be deduced that the extrusion barely
 440 modify sludge properties. The extruded samples still represent very well the original sludge.

441 With respect to the original sludge sample behavior, the apparent elastic modulus the intensely
 442 mixed sludge sample is unchanged. The threshold stress corresponding to the limit between the
 443 viscoelastic and the viscoplastic domains decreases from 4509 Pa to 3381 Pa (about 25.0% lower)
 444 while the permanent deformation is 7.2% higher, and, as expected, the maximum true stress
 445 measured at the end of the charging cycle is reduced by 22.7%. Mixing breaks the long polymeric
 446 chains (Charlou, 2014), therefore, a lower stress is required to get the same deformation in
 447 comparison to the original non-mixed sludge samples. From an energy point of view (see **Table 4**),
 448 the strain energy density u decreases with mixing while the ratio e increases. All in all, the absolute
 449 total amount of energy dissipated within the material is 17% lower for the mixed sample. Regarding
 450 the textural properties, mixing does not change the sludge cohesiveness, contrary to aging. This
 451 suggests that cohesiveness arises mainly from physical and chemical bonds at the floc’s scale. On the
 452 other hand, mixing increases significantly the adhesive stress and the energy of adhesion the
 453 material.

Mixing (min)	u (J/m ³)	e (-)	$\sigma_{ad,max}$ (Pa)	w_{ad} (10 ⁻⁶ J)	co (-)
0	1199 ± 40	81.5 ± 0.4%	248 ± 28	122.1 ± 15.4	39.33 ± 0.4%
5	1163 ± 60	82.4 ± 1.0%	8743 ± 23	1007.7 ± 419.8	39.86 ± 0.8%
20	964 ± 54	83.8 ± 0.7%	1264 ± 132	1618.8 ± 324.5	40.02 ± 0.5%

454

Table 4: Calculated textural properties of original and premixed sludge

455 In any case, the method is sensitive enough to reveal changes induced by structural changes in the
456 material.

457 **5 Conclusion**

458 An entire protocol of uniaxial compression tests is developed to characterize the complex transition
459 between solid and fluid states behavior of mechanically dewatered sewage sludge of TS≈20%. The
460 sample preparation by extrusion reduces the sludge heterogeneity and ensures the good
461 repeatability of mechanical tests. The single large strain (115%) compression serves to identify the
462 bioyield of the material; the sequential series of cyclic compressions are then limited up to the
463 previously identified bioyield (strain<0.21) with various operating conditions: compression speeds,
464 maximum deformations, destructured sludge and aged samples. With true stress-true strain plots, it
465 is illustrated that the viscoelastic behavior of sludge samples below yield stress and the plastic
466 deformations when exceeding the threshold. The rheological and textural properties of tested
467 samples are determined, and the impacts of destructure and biodegradation on the sludge behavior
468 is highlighted. This methodology revealed that the viscosity and the yield stress are the most sensible
469 rheological factors to operational conditions. To improve the flow control in processing, the
470 optimization handling should be focused on reducing these two factors. Aging and premixing can
471 decrease the yield stress and the viscosity of sludge, however, they increase accordingly the adhesive
472 effect of sludge. So, the characterization studies on the rheological and textural properties of sludge
473 are essential in process optimization.

474 The uniaxial compression test is proved to be an effective and sensitive characterizing method with
475 good repeatability and reproducibility. The identified rheological behaviors and the estimated
476 properties' values will be used for the following modelling and numerical simulation parts of our
477 characterization methodology. This methodology can be applied to characterize soft solid materials,
478 which do not flow under their own weight by gravity (higher than liquid limit) and, at the same time,
479 can be considered as continuous media (lower than plastic limit).

480 6 Bibliography

- 481 Agoda-Tandjawa, G., Dieudé-Fauvel, E., Girault R., and Baudez J.C., 2013. "Using Water Activity
482 Measurements to Evaluate Rheological Consistency and Structure Strength of Sludge."
483 *Chemical Engineering Journal* 228: 799–805.
- 484 Baroutian, S., Eshtiaghi, N., and Gapes D.J., 2013. "Rheology of a Primary and Secondary Sewage
485 Sludge Mixture: Dependency on Temperature and Solid Concentration." *Bioresource*
486 *Technology* 140: 227–33.
- 487 Battistoni, P., 1997. "Pre-Treatment, Measurement Execution Procedure and Waste Characteristics in
488 the Rheology of Sewage Sludges and the Digested Organic Fraction of Municipal Solid
489 Wastes." *Water Science and Technology*, Sludge Rheology Selected Proceedings of the
490 International Workshop on the Rheology of Sludges Sludge Management International
491 Specialized Conference on Sludge Management, 36 (11): 33–41.
- 492 Baudez, J.C., 2008. "Physical Aging and Thixotropy in Sludge Rheology." *Applied Rheology* 18 (1):
493 13495.
- 494 Baudez, J.C., and Coussot, P., 2001. "Rheology of Aging, Concentrated, Polymeric Suspensions:
495 Application to Pasty Sewage Sludges." *The Society of Rheology* 45 (5): 1123–39.
- 496 Baudez, J.C., Markis F., Eshtiaghi N., and Slatter P., 2011. "The Rheological Behaviour of Anaerobic
497 Digested Sludge." *Water Research* 45 (17): 5675–80.
- 498 Baudez, J.C., Slatter P, and Eshtiaghi N., 2013. "The Impact of Temperature on the Rheological
499 Behaviour of Anaerobic Digested Sludge." *Chemical Engineering Journal* 215–216 (January):
500 182–87.
- 501 Baudez, J.C., Coussot P., and Thirion F., 1998. "Rheology of sludge of Wastewater Treatment Plant:
502 Preliminary studies for mastering of storage and spreading." (in French, Rhéologie Des Boues
503 de Stations D'épuration : études Préliminaires Pour La Maîtrise Des Stockages et épandages.)
504 Ingénieries - EAT - N°15.
- 505 Beckley, J. and Banerjee, S., 1999. "Operational issues with impulse drying sludge." *Water Science &*
506 *Technology* 40 (11-12): 163–168.
- 507 Cai, W., McDowell G. R., and Airey G. D., 2013. "Discrete Element Modelling of Uniaxial Constant
508 Strain Rate Tests on Asphalt Mixtures." *Granular Matter* 15 (2): 163–74.
- 509 Chaari, F., Racineux G., Poitou R., and Chaouche M., 2003. "Rheological Behavior of Sewage Sludge
510 and Strain-Induced Dewatering." *Rheologica Acta* 42 (3): 273–79.
- 511 Charlou, C., 2014. "Characterization and modelling of sewage sludge flow in paddle dryer" (in French,
512 Caractérisation et modélisation de l'écoulement des boues résiduaire dans un sécheur à
513 palettes.), PhD. Thesis, Albi: Université de Toulouse.
- 514 Chhabra, R. P., and Richardson J. F., 2011. *Non-Newtonian Flow and Applied Rheology: Engineering*
515 *Applications*. Butterworth-Heinemann.
- 516 Coussot, P., 2014. "Yield Stress Fluid Flows: A Review of Experimental Data." *Journal of Non-*
517 *Newtonian Fluid Mechanics* 211 (September): 31–49.
- 518 Curvers, D., Saveyn H., Scales P. J., and Van der Meeren P., 2009. "A Centrifugation Method for the
519 Assessment of Low Pressure Compressibility of Particulate Suspensions." *Chemical*
520 *Engineering Journal* 148 (2–3): 405–13.
- 521 Dai, X., Gai X., and Dong B., 2014. "Rheology Evolution of Sludge through High-Solid Anaerobic
522 Digestion." *Bioresource Technology* 174: 6–10.
- 523 Dusserre, G., Bernhart G., Schmidt F. M., and Dour G., 2011. "Evaluation of Viscous and Elastic
524 Parameters of a Borosilicate Glass above Transition Temperature Using Optical Instrumented
525 Squeeze Tests." *Journal of Non-Newtonian Fluid Mechanics* 166 (21–22): 1229–38.
- 526 Eshtiaghi, N., Markis F., Dong Yap S., Baudez J.C., and Slatter P., 2013. "Rheological Characterisation
527 of Municipal Sludge: A Review." *Water Research* 47 (15): 5493–5510.
- 528 Farno, E., Baudez J.C., Parthasarathy R., and Eshtiaghi N., 2014. "Rheological Characterisation of
529 Thermally-Treated Anaerobic Digested Sludge: Impact of Temperature and Thermal History."
530 *Water Research* 56: 156–61.

531 Feng, G., Liu L., and Tan W. 2014. "Effect of Thermal Hydrolysis on Rheological Behavior of Municipal
532 Sludge." *Industrial & Engineering Chemistry Research* 53 (27): 11185–92.

533 G'sell, C. and Jonas J. J., 1979. "Determination of the Plastic Behaviour of Solid Polymers at Constant
534 True Strain Rate." *Journal of Materials Science* 14 (3): 583–91.

535 Hort, J., Grys, G., and Woodman, J., 1997. "The relationships between the chemical, rheological and
536 textural properties of Cheddar cheese." *Le lait* 77 (5): 587–600.

537 Jiang, J., Wu J., Poncin S., and Li H., 2014. "Rheological Characteristics of Highly Concentrated
538 Anaerobic Digested Sludge." *Biochemical Engineering Journal* 86: 57–61.

539 Jing, S.R., Lin, Y.F., Lin, Y.M., Hus, C.S., Huang, C.S., and Lee, D.Y., 1999. "Evaluation of effective
540 conditioners for enhancing sludge dewatering and subsequent detachment from filter cloth."
541 *Journal of Environmental Science and Health Part A* 34(7): 1517–1531.

542 Johnson, K. L., Kendall K., and Roberts A. D., 1971. "Surface Energy and the Contact of Elastic Solids."
543 *Proceedings of the Royal Society of London A: Mathematical, Physical and Engineering*
544 *Sciences* 324 (1558): 301–13.

545 Kudra, T., 2003. "Sticky Region in Drying—Definition and Identification." *Drying Technology* 21 (8):
546 1457–69.

547 Li, B., Wang, F., Chi, Y., and Yan. J.H., 2014. "Adhesion and Cohesion Characteristics of Sewage Sludge
548 During Drying." *Drying Technology* 32 (13): 1598–1607.

549 Liang, F., Chen X., Mao H., Sauceau M., Arlabosse P., Wang F., and Chi Y., 2016. "The Microstructure:
550 A Critical Factor In Characterising The Sticky Properties Of Highly Concentrated Sewage
551 Sludge." *6th International Conference on Engineering for Waste and Biomass Valorisation*.

552 Lin, Y. M., Sharma P. K., and van Loosdrecht M. C. M., 2013. "The Chemical and Mechanical
553 Differences between Alginate-like Exopolysaccharides Isolated from Aerobic Flocculent
554 Sludge and Aerobic Granular Sludge." *Water Research* 47 (1): 57–65.

555 Lotito, V., and Lotito A. M., 2014. "Rheological Measurements on Different Types of Sewage Sludge
556 for Pumping Design." *Journal of Environmental Management* 137: 189–96.

557 Markis, F., Baudez J.C., Parthasarathy R., Slatter P., and Eshtiaghi N., 2014. "Rheological
558 Characterisation of Primary and Secondary Sludge: Impact of Solids Concentration." *Chemical*
559 *Engineering Journal* 253 (October): 526–37.

560 Ma, Y., Xia C., Yang H., and Zeng R. J., 2014. "A Rheological Approach to Analyze Aerobic Granular
561 Sludge." *Water Research* 50 (March): 171–78.

562 Mohsenin, N. N., 1984. *Physical Properties of Food and Agriculture Materials : A Teaching Manual*.
563 New York: Gordon and Breach Science Publishers.

564 Mori, M., Isaac J., Seyssiecq I., and Roche N., 2008. "Effect of Measuring Geometries and of
565 Exocellular Polymeric Substances on the Rheological Behaviour of Sewage Sludge." *Chemical*
566 *Engineering Research and Design*, 11th Congress of the French Chemical Engineering Society,
567 86 (6): 554–59.

568 Mori, M., Seyssiecq I., and Roche N., 2006. "Rheological Measurements of Sewage Sludge for Various
569 Solids Concentrations and Geometry." *Process Biochemistry* 41 (7): 1656–62.

570 Nielsen, P., Frolund B., and Keiding K., 1996. "Changes in the Composition of Extracellular Polymeric
571 Substances in Activated Sludge during Anaerobic Storage." *Applied Microbiological*
572 *Biotechnology* 44.

573 Ohm, T.-I., Chae, J.-S., Kim, J.-E., Kim, H., and Moon, S.-H., 2009. "A study on the dewatering of
574 industrial waste sludge by fry-drying technology." *Journal of Hazardous Materials* 168 (1):
575 445–450.

576 O'Kelly, B. C., 2005. "Mechanical Properties of Dewatered Sewage Sludge." *Waste Management* 25
577 (1): 47–52.

578 O'Kelly, B. C., 2006. "Geotechnical properties of municipal sewage sludge." *Geotechnical and*
579 *Geological Engineering*, no. 24: 833–50.

580 O'Kelly, B. C., 2008. "Effect of Biodegradation on the Consolidation Properties of a Dewatered
581 Municipal Sewage Sludge." *Waste Management* 28 (8): 1395–1405.

582 Papadakis, S.E. and Bahu, R.E., 1992. "The Sticky Issues of Drying." *Drying Technology* 10 (4): 817–
583 837.

584 Pelletier, A., Worcel A., and Terver S., 1998. "Design, Realisation and Validation of a Non-Destructive
585 Cyclical Uniaxial Mechanical Compression Test." *Journal of Biomechanics*, Proceedings of the
586 11th Conference of the European Society of Biomechanics, 31, Supplement 1: 136.

587 Peeters, B., Dewil, R., Van Impe, J.F., Vernimmen, L., and Smets, I.Y., 2010. "Using a Shear Test Based
588 Lab Protocol to Map the Sticky Phase of Activated Sludge." *Environmental Engineering
589 Science* 28 (1): 81–85.

590 Pevere, A., Guibaud G., Goin E., Van Hullebusch E., and Lens P., 2009. "Effects of Physico-Chemical
591 Factors on the Viscosity Evolution of Anaerobic Granular Sludge." *Biochemical Engineering
592 Journal* 43 (3): 231–38.

593 Ramírez-Wong, B., Sweat V. E., Torres P. I., and Rooney L. W., 1996. "Evaluation of the Rheological
594 Properties of Fresh Corn Masa Using Squeezing Flow Viscometry: Biaxial Extensional
595 Viscosity1." *Journal of Texture Studies* 27 (2): 185–98.

596 Ratkovich, N., Horn W., Helmus F. P., Rosenberger S., Naessens W., Nopens I., and Bentzen T. R.,
597 2013. "Activated Sludge Rheology: A Critical Review on Data Collection and Modelling."
598 *Water Research* 47 (2): 463–82.

599 Roudot, A. C. 2002. Rheology and analysis of food texture (in French, Rhéologie et analyse de texture
600 des aliments.) Paris: TEC & DOC.

601 Ruiz, T., Kaosol T., and Wisniewski C., 2010. "Dewatering of Urban Residual Sludges: Filterability and
602 Hydro-Textural Characteristics of Conditioned Sludge." *Separation and Purification
603 Technology* 72 (3): 275–81.

604 Ruiz, T., and Wisniewski C., 2008. "Correlation between Dewatering and Hydro-Textural
605 Characteristics of Sewage Sludge during Drying." *Separation and Purification Technology* 61
606 (2): 204–10.

607 Ségalen, C., Dieudé-Fauvel E., and Baudez J.C., 2015. "Electrical and Rheological Properties of Sewage
608 Sludge – Impact of the Solid Content." *Water Research*, Special Issue on Sludge Research, 82
609 (October): 25–36.

610 Seyssiecq, I., Ferrasse J.H., and Roche N., 2003. "State-of-the-Art: Rheological Characterisation of
611 Wastewater Treatment Sludge." *Biochemical Engineering Journal* 16 (1): 41–56.

612 Sharma, P. K., H. J. Busscher, T. Terwee, S. A. Koopmans, and T. G. van Kooten. 2011. "A Comparative
613 Study on the Viscoelastic Properties of Human and Animal Lenses." *Experimental Eye
614 Research* 93 (5): 681–88.

615 Sharma, S., and Bhattacharya S., 2014. "Strain and Strain Rate Dependence of Gellan, Agar and Agar–
616 gellan Gels as Model Systems." *Journal of Food Engineering* 141 (November): 93–98.

617 Steffe, J., 1996. *Rheological Methods in Food Process Engineering*. USA: Freeman Press.

618 Sveegaard, S.G., Keiding, K., and Christensen, M.L., 2012. "Compression and swelling of activated
619 sludge cakes during dewatering." *Water Research* 46 (16): 4999–5008.

620 Wolny, L., Wolski P., and Zawieja I., 2008. "Rheological Parameters of Dewatered Sewage Sludge
621 after Conditioning." *Desalination*, European Desalination Society and Center for Research
622 and Technology Hellas (CERTH), Sani Resort 22 –25 April 2007, Halkidiki, Greece European
623 Desalination Society and Center for Research and Technology Hellas (CERTH), Sani Resort,
624 222 (1–3): 382–87.

625 Yen, P.S., Chen L.C., Chien C.Y., Wu R.M., and Lee D. J., 2002. "Network Strength and Dewaterability
626 of Flocculated Activated Sludge." *Water Research* 36 (3): 539–50.

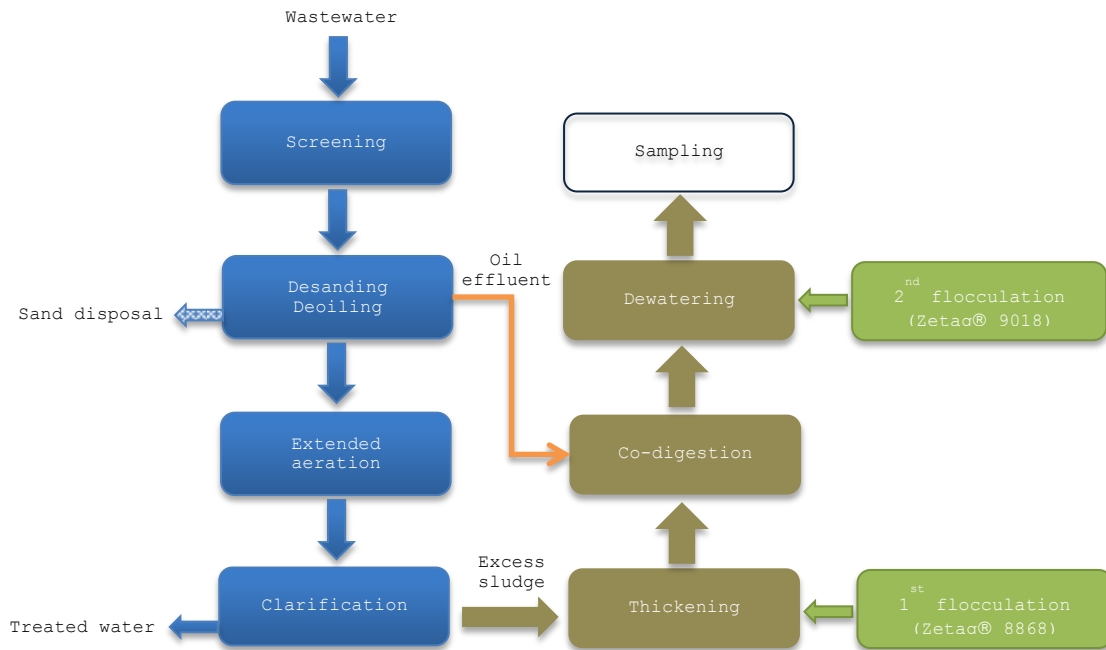
627 Yu, J., Santos P.H.S., and Campanella O.H., 2012. "A Study to Characterize the Mechanical Behavior of
628 Semisolid Viscoelastic Systems Under Compression Chewing – Case Study of Agar Gel." *629 Journal of Texture Studies* 43 (6): 459–67.

630 Zhang, C., Cao P., Pu C., Liu J., and Wen P., 2014. "Integrated Identification Method of Rheological
631 Model of Sandstone in Sanmenxia Bauxite." *Transactions of Nonferrous Metals Society of
632 China* 24 (6): 1859–65.

633

635

636



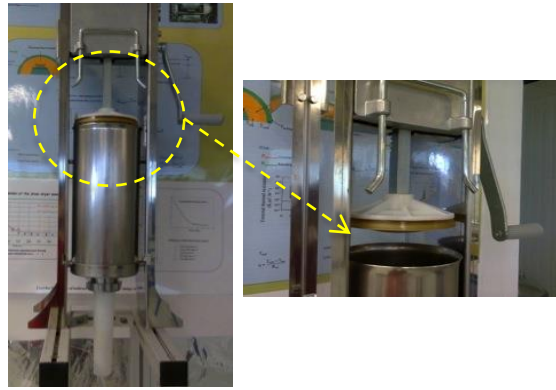
637

638 **Figure 1:** Municipal wastewater treatment process at Albi WWTP, the location of the mechanically
639 dewatered sludge samples collected for rheological characterisation

640

641

642
643



(a)



(b)

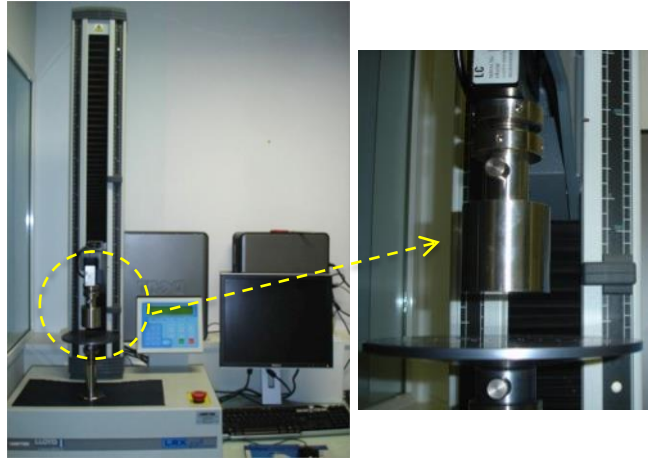


(c)

644
645
646
647

Figure 2: (a) Manual extruder (b) Original sludge samples before shaping (c) Extruded sludge sample

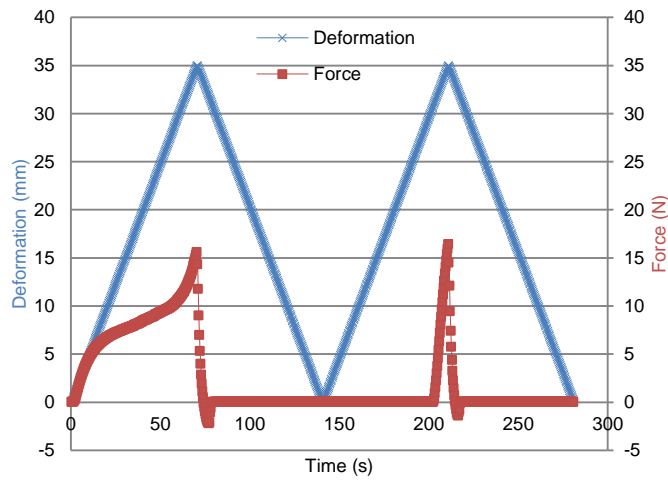
648
649
650
651



652
653
654
655

Figure 3: Universal testing machine

656



657

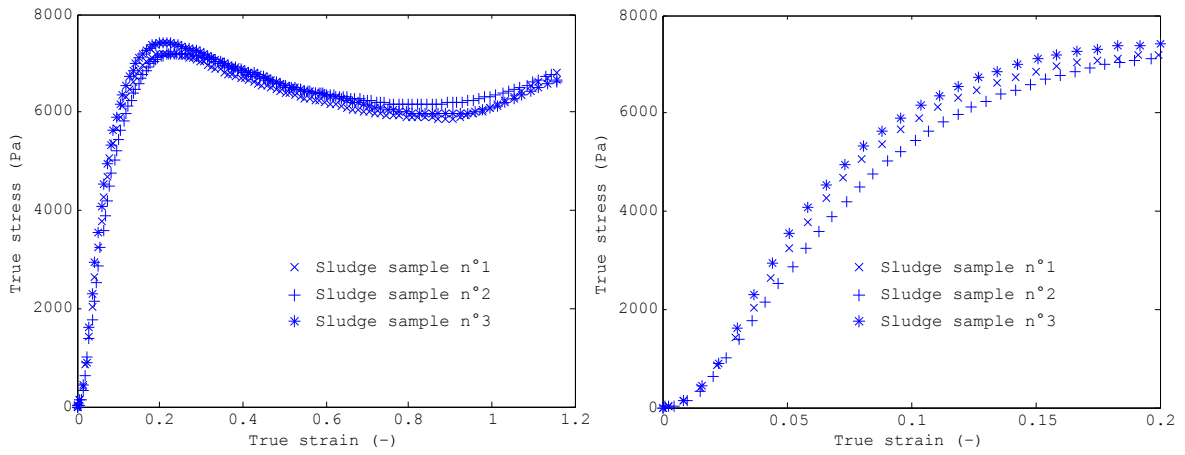
658

Figure 4: Mechanical response to a uniaxial cyclical compression test with $\Delta h_{\max}=35\text{mm}$ and $V=0.5\text{mm/s}$

659

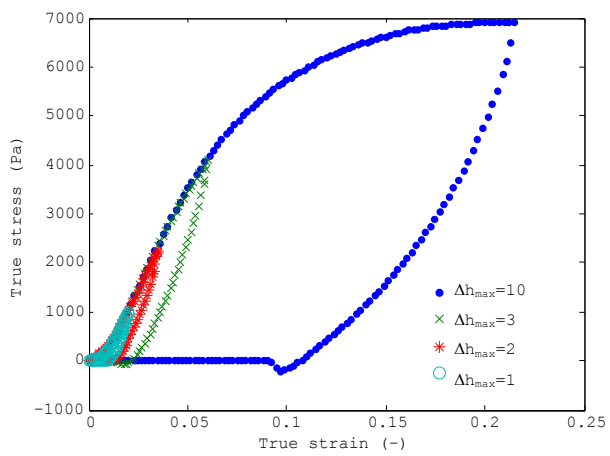
660

661

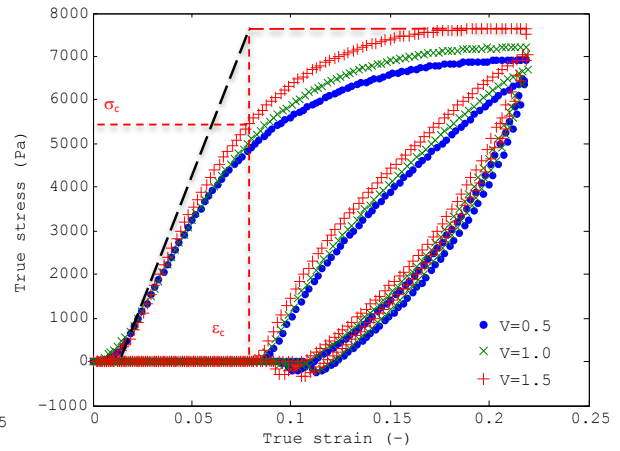


(a)

(b)



(c)



(d)

Figure 5: (a) Single compression curves for 3 identical fresh raw sludge samples with $\Delta h_{\max}=35$ mm and $V=0.5$ mm/s; (b) zoomed out curves ($0 < \varepsilon < 0.2$) in (a); (c) 1 cycle compression tests on 4 identical original sludge with $V=0.5$ mm/s and $\Delta h_{\max}=1, 2, 3$ and 10 mm; (d) 2 consecutive cycles compression tests on 3 identical original sludge with $\Delta h_{\max}=10$ mm and $V=0.5, 1.0$ and 1.5 mm/s, and estimation of yield stress σ_c and strain ε_c (using regressed lines for ideal elastic and plastic behaviors)

662
663

664



(a)

(b)

(c)

665

666

667

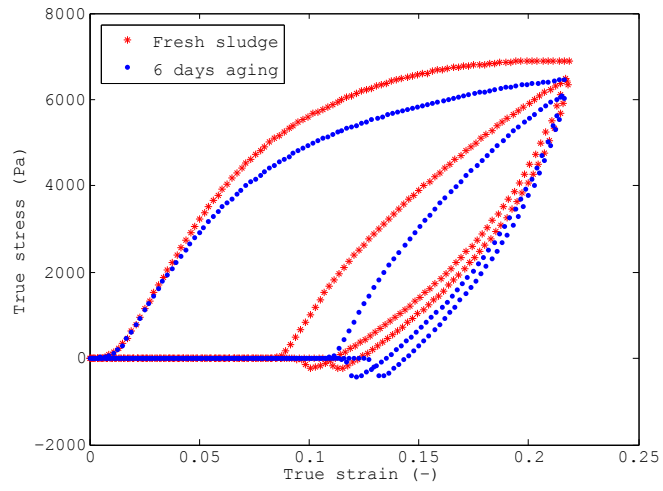
668

669

Figure 6: (a) Non-fractured sludge sample after compression test; (b) tested sludge sample cut into slice for internal crack detection: no internal fracture observed; (c) fractured sludge sample after compression test

670

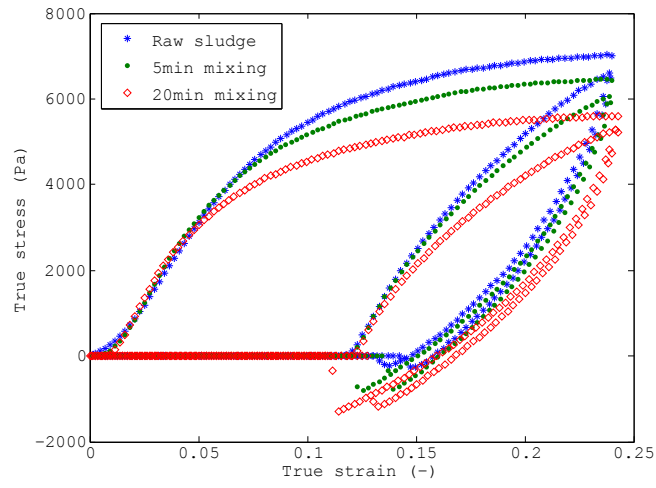
671



672
 673
 674
 675

Figure 7: Influence of aging on sludge behavior with $\Delta h_{\max}=10\text{mm}$ and $V=0.5\text{ mm/s}$

676



677

678

Figure 8: Influence of premixing on sludge behavior with $\Delta h_{\max}=10\text{mm}$ and $V=0.5\text{ mm/s}$

679

680